ORIGINAL RESEARCH

Angesinenolide B, A Phthalide Dimeric Peroxide, Exerts Anti-Inflammatory Properties by Suppressing MAPK/STATs Signaling Pathways and ROS Production

Laibin Zhang, Yuan Liu, Huanhuan Wang, Shuangyan Guo, Jieli Lv

School of Pharmacy, Xinxiang Medical University, Xinxiang, Henan, 453003, People's Republic of China

Correspondence: Laibin Zhang; Jieli Lv, School of Pharmacy, Xinxiang Medical University, 601 Jinsui Road, Xinxiang, Henan, 453003, People's Republic of China, Email zhanglb@xxmu.edu.cn; jielilv2009@xxmu.edu.cn

Purpose: Angesinenolide B (ASB), a phthalide dimer with a peroxy bridge, is uniquely isolated from Chinese medicine *Angelica sinensis* radix and demonstrates significant anti-inflammatory properties. The objective of the current study was to evaluate the anti-inflammatory function of ASB and the potential mechanism in lipopolysaccharide (LPS)-stimulated macrophages and $CuSO_4$-induced zebrafish models.
Methods: The level of nitric oxide (NO), a proinflammatory mediator, in LPS-stimulated RAW264.7 cells was quantified using Griess method. ELISA was employed to investigate the generation of tumor necrosis factor-α (TNF-α) and interleukin-6 (IL-6), while qRT-PCR was utilized to analyze the mRNA expressions of TNF-α, IL-6, inducible NO synthase (iNOS) and cyclooxygenase-2 (COX-2). Fluorescence microscopy and flow cytometry were employed for the determination of ROS generation. Western blot and immuno-fluorescence techniques were utilized to assess the impact of ASB on iNOS and COX-2, and on the NF-κB, MAPK and STATs signaling pathways. Moreover, the affinities between ASB and the target proteins were verified by molecular docking analysis. In vivo, ROS generation was explored using fluorescent probe DCFH-DA, and the TNF-α and IL-6 mRNA expressions were also evaluated in $CuSO_4$-induced zebrafish inflammation model.
Results: ASB treatment was found to suppress the levels of NO, TNF-α, IL-6 and ROS, restrain the expressions of iNOS and COX-2 proteins and mRNA, as well as down-regulate MAPK and STATs signaling pathways in LPS-stimulated RAW264.7 cells. Furthermore, the administration of ASB effectively attenuated the overproduction ROS and the high mRNA expressions of TNF-α and IL-6 in a zebrafish model of inflammation induced by $CuSO_4$.
**Conclusion:** ASB has the potentiality to reduce the levels of proinflammatory mediators and cytokines, decrease ROS production, and also down-regulate the MAPK and STATs signaling pathways, thereby exerting an anti-inflammatory effect. This implies that ASB could potentially serve as a viable approach for addressing inflammatory conditions.
Keywords: Angesinenolide B, anti-inflammation, signaling pathway, cytokine, ROS

Introduction

Inflammation serves as the body's essential physiological defense mechanism, yet excessive inflammation can contribute to a spectrum of illnesses. Macrophages take a pivotal role in the process of inflammation. Activated by damage factors, macrophages secrete substantial quantities of inflammatory mediators and factors, such as nitric oxide (NO), tumor necrosis factor-α (TNF-α) and interleukin 6 (IL-6). The potent macrophage activator, lipopolysaccharide (LPS), triggers the inflammatory response via a signaling pathway network.[1,2] The classical signaling pathways of inflammation, including nuclear factor κB (NF-κB), mitogen-activated protein kinase (MAPK) and signal transducer and activator of transcription (STATs) signaling pathways, facilitate the initiation of inflammatory response through regulating the phosphorylation of diverse effector molecules.[3,4] Therefore, the suppression of excessive generation of proinflammatory

1557

Graphical Abstract
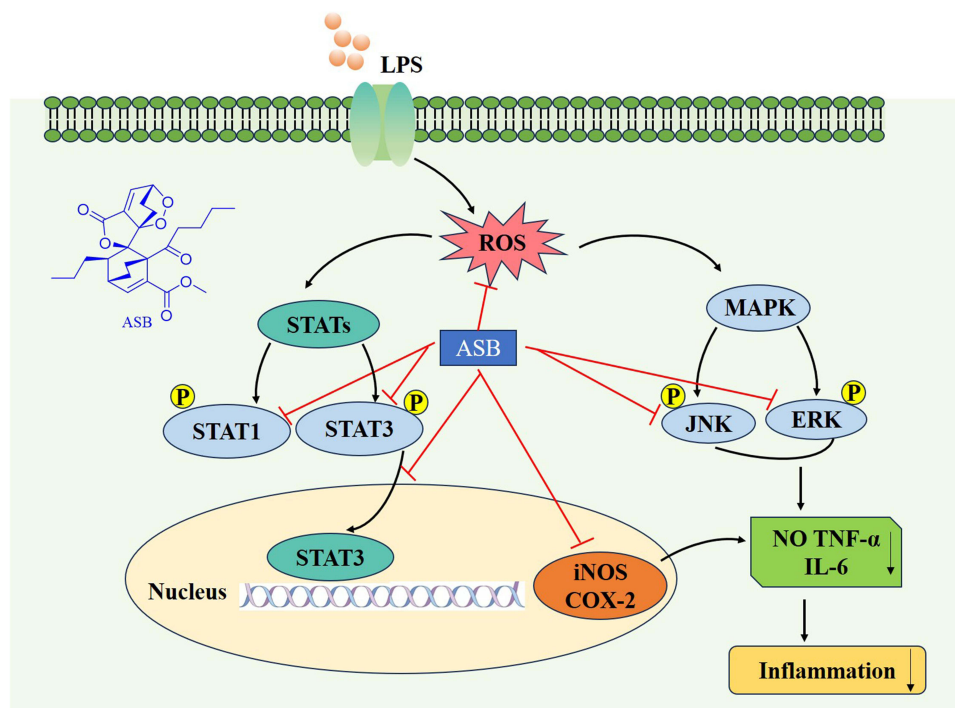
mediators or cytokines, coupled with the modulation of inflammation signaling pathways, could be considered a hopeful treatment for managing inflammatory diseases.

The zebrafish, a small teleost, is extensively employed as an economical and suitable model for investigating physiological and pharmacological approaches of human disease due to its high genomic similarity to humans, as well as its diminutive size, rapid growth rate, and transparent embryos.[5,6] The utilization of zebrafish as an animal model for the study of inflammation originated in the 2000s and has achieved rapid development. Modeling inflammatory illnesses in zebrafish presents a significant potential as an invaluable tool for assessing novel anti-inflammatory compounds.[7]

Phthalides, a prominent group of biologically active natural compounds, are extensively present in plants, fungi, and lichens. They occupy a cumulatively prominent position as a result of their varied biological activities and intricate chemical structures.[8] In recent years, some natural phthalides with unique structures have been extracted from traditional Chinese medicine, exhibiting significant anti-inflammatory characteristics.[9–11]

Angelica sinensis radix is frequently utilized in Chinese medicine and nutritional food supplements in China, renowned for its ability to enhance blood circulation and relieve pain. Phthalides have been recognized as the primary biochemical and pharmacological active constituent of *A. sinensis* radix, which exerts a diverse array of biological functions including anti-inflammatory, anticoagulation, anti-tumor, analgesic and neuroprotective effects.[12] Angesinenolide B (ASB), an unparalleled phthalide dimer peroxy compound with anticoagulant activity (Figure 1), which had been isolated from *A. sinensis* radix by our research group.[13] Recently, our further study found that it also possessed remarkable anti-inflammatory activity. However, no research has examined the anti-inflammatory effect of ASB so far. In the current investigation, ASB was assessed for its anti-inflammatory properties utilizing the NO generation model in LPS-induced RAW 264.7 macrophages, and further investigations were conducted to clarify the underlying molecular mechanism. The application of the molecular docking method to verify the binding effects of drugs and potential targets can provide insights into the potential therapeutic effects of drugs on diseases. Therefore, the
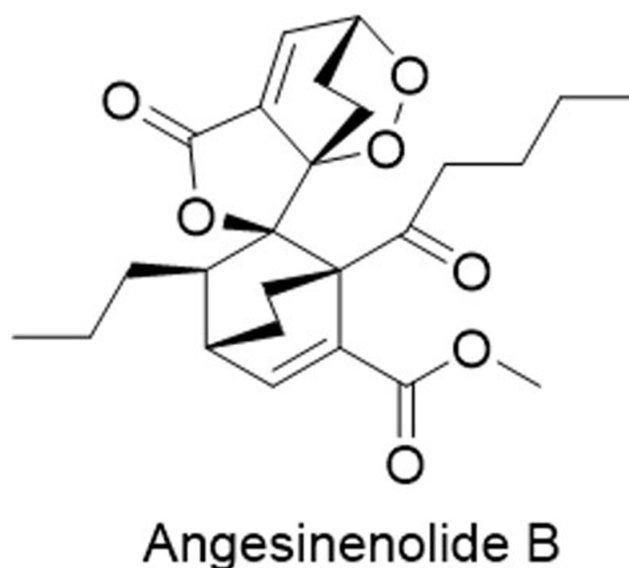
Figure 1 The chemical structure of ASB.

molecular docking technique was employed to analyze the binding ability of ASB to potential targets. Additionally, the in vivo anti-inflammatory efficacy of ASB was further evaluated utilizing a zebrafish model.

Material and Methods

Reagents

ASB was obtained from *Angelica sinensis* radix as previously described[13] and its purity was measured using HPLC, with a purity exceeding 98%. Dulbecco's modified Eagle's medium (DMEM) was acquired from BasalMedia (Shanghai, China). Fetal bovine serum (FBS) was obtained from Gemini (Woodland, CA, USA). Methylthiazolyldiphenyl-tetrazolium Bromide (MTT) was acquired from MP Biochemicals (CA, USA). TNF-α ELISA Kits were purchased from NeoBioscience (Shenzhen, China). IL-6 ELISA Kits and Alexa Fluor 488-labeled goat anti-rabbit IgG antibody were purchased from Boster (Wuhan, China). HRP-labeled secondary goat anti-rabbit antibody was obtained from Beyotime (Shanghai, China). LPS from *Escherichia coli* O55:B5 were provided by Sigma (St. Louis, MO, USA). Inducible nitric oxide synthase (iNOS) (Cat# 13120S), cyclooxygenase-2 (COX-2) (Cat# 12282S), p38 (Cat# 8690S), *p*-p38 (Cat# 4511S), ERK1/2 (Cat# 4695S), *p*-ERK1/2 (Cat# 4370S), JNK (Cat# 9252S), *p*-JNK (Cat# 4668S), p65 (Cat# 8242S), *p*-p65 (Cat# 3033S), IκBα (Cat# 4814S), *p*-IκBα (Cat# 2859S), STAT1 (Cat# 14994T), *p*-STAT3 (Cat# 9145T) antibodies were acquired from Cell Signaling Technology (Danvers, MA, USA). *p*-STAT1 (Cat# AF3300), STAT3 (Cat# AF6295), *p*-AKT (Cat# AF0016), GAPDH (Cat# AF7021), *β*-actin (Cat# AF7018), Tubulin (Cat# AF7011) antibodies were acquired from Affinity Biosciences (Cincinnati, OH, USA). AKT (Cat# P42574) antibody was obtained from Abways Technology (Shanghai, China). Quercetin standard with a purity exceeding 98% was acquired from National Institutes for the Control of Pharmaceutical and Biological Products (Beijing, China). TNF-α, IL-6, iNOS, COX-2, GAPDH and *β*-actin primers were purchased from Sangon Biotech (Shanghai, China). $CuSO_4$ was acquired from Sinopharm Chemical Reagent (Shanghai, China). H2DCFDA was purchased from MedChemexpress (NJ, USA).

Cell Culture

RAW 264.7 cells were procured from Procell Life Science & Technology Co. Ltd (Wuhan, China). The cells were cultivated in DMEM containing 10% FBS and 1% double-antibody (100 U/mL penicillin and 100 μg/mL streptomycin) and incubated in an incubator with 5% CO_2 at 37°C.

Cell Viability Assay

Cell viability was assessed using the MTT assay, following previously established protocols.[14,15] In short, RAW 264.7 cells (5×10^4 cells/well) were seeded in a 96-well plate and cultured for 24 h. Subsequently, they were pre-treated with LPS (1 μg/mL) and ASB or quercetin for the following 16 h. After the removal of the medium from the wells, an addition of MTT solution (0.5 mg/mL) was carried out and cultured for 4 h. Finally, the supernatant was discarded and 150 μL of DMSO was added to each well for solubilization with gentle horizontal shaking. The absorbance was quantified at 570 nm utilizing a microplate reader. Each trial was conducted in triplicate.

NO Measurement

The level of NO was assessed using the Griess assay. RAW264.7 cells (1.5×10^5 cells/well) were plated into 96-well plates and cultured for 24 h. The cells were subsequently exposed to LPS (1 μg/mL) in the presence or absence of ASB (2–10 μM) or quercetin (10–70 μM) for a duration of 16 h. The supernatant (50 μL) was combined with an equal volume of Griess I reagent (50 μL) and Griess II reagent (50 μL) and oscillated for 10 min, followed by measurement of the absorbance at 540 nm. The concentration of NO was calculated according to the standard calibration curve, and the 50% inhibition concentration (IC_{50}) was determined. Quercetin was employed as a positive control in the experiment.

Cytokines Assay in RAW 264.7 Cells

RAW 264.7 cells were plated at 1.5×10^5 cells per well into 96-well plates and incubated for 24 h. Then, the cells were pre-treated with LPS (1 μg/mL) and with or without ASB at concentrations of 2, 6 and 10 μM for an additional 16 h. The levels of TNF-α and IL-6 in the cellular supernatants were quantified utilizing ELISA kits following the specifications offered by the manufacturer.

Quantitative Real-Time Polymerase Chain Reaction (qRT-PCR)

RAW 264.7 macrophages (3×10^6 cells/well in a 6-well plate) were stimulated using LPS (1 μg/mL) with or without ASB for 16 h. Subsequently, total RNA was extracted from the cells utilizing Trizol reagent (Accurate Biotechnol, Hunan, China). The concentration and purity of RNA were assessed utilizing a NanoPhotometer N60 spectrophotometer. The 2 μg of total RNA was subjected to reverse transcription to generate cDNA utilizing the All-in-One Script RT Premix Kit (Kermey, Zhengzhou, China). The cDNA templates were amplified and quantified using the SYBR kit (Kermey, Zhengzhou, China) according to the following PCR reaction: an initial denaturation at 95°C for 30s, followed by 40 cycles of 95°C for 10s and 60°C for 10s. The relative expression levels of TNF-α, IL-6, COX-2 and iNOS mRNA were determined by normalizing to the level of GAPDH in the same cDNA utilizing the $2^{-\Delta\Delta CT}$ method for relative quantification. The PCR primer sequences were documented in Table 1.

Table I List of qRT-PCR Primer

Model	Gene	Primer	Sequence
Macrophage	TNF-α	Forward	5′-CTTGTTGCCTCCTCTTTTGCTTA-3′
		Reverse	5′-CTTTATTTCTCTCAATGACCCGTAG-3′
	IL-6	Forward	5′-AAGGAGTGGCTAAGGACCAAGAC-3′
		Reverse	5′-AGTGAGGAATGTCCACAAACTGATA-3′
	iNOS	Forward	5′-GAATCTTGGAGCGAGTTGTGGA-3′
		Reverse	5′-GTGAGGGCTTGGCTGAGTGAG-3′
	COX-2	Forward	5′-CTGGTGCCTGGTCTGATGATGT-3′
		Reverse	5′-AGTCTGCTGGTTTGGAATAGTTGCT-3′
	GAPDH	Forward	5′-CTTTGGCATTGTGGAAGGGCTC-3′
		Reverse	5′-GCAGGGATGATGTTCTGGGCAG-3′

(Continued)

Table I (Continued).

Model	Gene	Primer	Sequence
Zebrafish	TNF-α	Forward	5'-GCTGGATCTTCAAAGTCGGGTGTA-3'
		Reverse	5'-TGTGAGTCTCAGCACACTTCCATC-3'
	IL-6	Forward	5'-GTCTGCTACACTGGCTACACTCTTC-3'
		Reverse	5'-CGTCCACATCCTGAACTTCGTCTC-3'
	β-actin	Forward	5'-AGAGCTATGAGCTGCCTGACG-3'
		Reverse	5'-CCGCAAGATTCCATACCCA-3'

ROS Assay in RAW 264.7 Cells

RAW 264.7 cells were cultured in a 6-well plate (6×10^5 cells/well) and cultured for 24 h. After that, the cells were exposed to LPS (1 μg/mL) and with or without ASB (2, 6, 10 μM) for durations of 20 h. The supernatant was aspirated, and the cells were rinsed with medium. Subsequently, 1 mL of 10 μM H2DCFDA was added, followed by incubation of the cells at 37°C for 30 min. Fluorescence microscopy was employed to capture images. Additionally, cells were inoculated at a 2×10^6 cells per well in a six-well plate and subsequently subjected to the aforementioned treatment. Following incubation with 10 μM H2DCFDA, the cells were evaluated utilizing flow cytometry with the FlowJo software (Luminex, Guava easyCyte, USA).

Western Blot Analysis

RAW 264.7 cells were cultured in a 6-well plate (3×10^6 cells/well). After 24 h of incubation, the cells were exposed to LPS (1 μg/mL) and with or without ASB (2, 6, 10 μM) for durations of 15 min, 30 min, 6 h or16 h. Cellular proteins were extracted utilizing radio immunoprecipitation assay (RIPA) lysis buffer. The protein concentrations were quantified utilizing the bicinchoninic acid (BCA) protein assay kit (Beyotime, Shanghai, China). They were then separated using sodium dodecyl sulfate (SDS)-polyacrylamide gels electrophoresis (PAGE) and subsequently transferred onto polyvinylidene difluoride (PVDF) membranes. The membranes were closed for 2 h with 5% non-fat milk, and then underwent primary antibody incubation at 4°C overnight. Subsequently, the membrane was subjected to three washes with TBST (Tris-buffered saline solution containing 0.1% Tween 20) and then incubated using the secondary horseradish peroxidase (HRP)-labeled antibody for 2 h. After undergoing three additional washes with TBST, the membranes were visualized utilizing an enhanced chemiluminescence (ECL) reagent (Kemix, Beijing, China). The blot images were subjected to analysis with ImageJ software (NIH, Bethesda, MD, USA).

Immunofluorescence Analysis

Briefly, 96-well plates were plated with the RAW 264.7 cells (5×10^4 cells/well). After being cultured for 24 h, the cells were pre-treated with LPS (1 μg/mL) and with or without ASB (10 μM) for 6 h. The cells were rinsed thrice with PBS, immobilized using 4% paraformaldehyde for 20 min, and subsequently permeabilized using ice-cold methanol for 5 min at −20°C. Subsequently, the cells were closed with 5% BSA for 40 min, followed by incubation using the STAT3 primary antibody at 4°C overnight. After washing thrice with PBS, cells were labeled using a secondary antibody (Alexa Fluor 488-labeled Goat Anti-Rabbit IgG) for 1 h at 37°C in the absence of light. After being cleaned with PBS, the cells were stained using DAPI (5 μg/mL) for 5 min in the absence of light. Fluorescence microscopy was used to take images.

Molecular Docking Analysis

The crystal structure of the target proteins ERK1, ERK2, JNK, STAT1 and STAT3 were retrieved from RSCB protein database (https://www.rcsb.org/) for use in this study. The ASB structure was constructed using ChemDraw software and then converted from SDF to PDB format. ASB and the target proteins were designated as the ligand and receptors, respectively. The protein receptors were subsequently imported into AutoDock Tools (version 1.5.7) with the addition of hydrogen atoms, charge assignment, and removal of water molecules. Molecular docking was conducted applying

AutoDock Vina software to assess the affinity of the ligand and receptors, as well as the energy value. The visualization of molecular docking results was achieved using PyMOL software (version 2.5.0). The docking was deemed successful if the binding energy was less than −5.0 kcal/mol.

Zebrafish Maintenance

Zebrafish embryos were provided by Nanjing Ezerinka Biotechnology and maintained in standard E3 medium for culture. In all following tests, zebrafish at 3 days post-fertilization (dpf) were chosen as the subjects for the experiment. The tests carried out on zebrafish were authorized by the Animal Experimental Ethical Inspection of Xinxiang Medical University, with Approval ID Number: XYLL-20230066.

Toxicity of ASB in Zebrafish

Zebrafish larvae (3 dpf) were distributed into a 12-well plate through random allocation (n = 30) and subsequently subjected to varying concentrations of ASB (10, 20 and 30 μM). The culture medium was replaced on a daily basis, and deceased larvae were documented and taken out every 24 h until 8 dpf.

Measurement of ROS in CuSO$_4$-Induced Zebrafish

The determination of ROS in zebrafish was conducted utilizing the fluorescent probe H2DCFDA.[16] Zebrafish larvae (3 dpf) were randomly distributed into a 12-well plate at 20 larvae per well and subjected to pretreatment with ASB (10, 20 and 30 μM) for 1 h. ASB was subsequently rinsed and substituted with a 20 μM solution of CuSO4 for a duration of 20 min. The control group received treatment with E3 medium exclusively, whereas the model group was subjected to CuSO$_4$ (20 μM) for 20 min. After being rinsed three times with fresh E3 medium, zebrafish were exposed to H2DCFDA for 1 h at 28°C in the absence of light. Eventually, zebrafish larvae were subjected to fluorescence microscopy using a Zeiss microscope (Oberkochen, Germany), followed by quantification of fluorescence intensity utilizing ImageJ software.

Analysis of the mRNA Expressions of Pro-Inflammatory Cytokines in CuSO$_4$-Induced Zebrafish

Zebrafish larvae (3 dpf) were transplanted into a 12-well plate, with 20 larvae per well. Subsequently, the drug groups were exposed to varying concentrations of ASB (10, 20 and 30 μM) for 1 h. After pretreatment, the drug group and the model group underwent additional treatment with CuSO$_4$ (20 μM) for 4 h. Total RNA was extracted from the larvae utilizing Trizol reagent and was sampled for qRT-PCR analysis. The *β*-actin gene was employed as an internal reference, with the specific primer pairs utilized being detailed in Table 1.

Statistical Analysis

All data were presented as mean ± standard deviation (SD) (n = 3). Statistical analyses were conducted utilizing GraphPad Prism 7.0 software (San Diego, CA, USA). One-way ANOVA with a post-hoc Dunnett′s test was employed to evaluate the statistically significant values, with a level of $P < 0.05$ regarded as statistically significant.

Results
ASB Suppressed the LPS-Induced NO Production

In order to investigate the anti-inflammatory properties of ASB, NO production was determined in the LPS-induced RAW 264.7 cells. The results exhibited that ASB (2–10 μM) restrained the LPS-induced NO generation in a dose-dependent manner with IC$_{50}$ value at 4.98 ± 0.94 μM (positive control quercetin with an IC$_{50}$ value of 26.06 ± 2.28 μM) (Figure 2A and B). Meanwhile, ASB did not impact the viability of RAW 264.7 cells as assessed by the MTT assay at concentrations ranging of 2–10 μM, indicating that its inhibitory action was not associated with cytotoxicity to the cells. Similarly, quercetin exhibited no impact on cell viability at the measured concentrations.
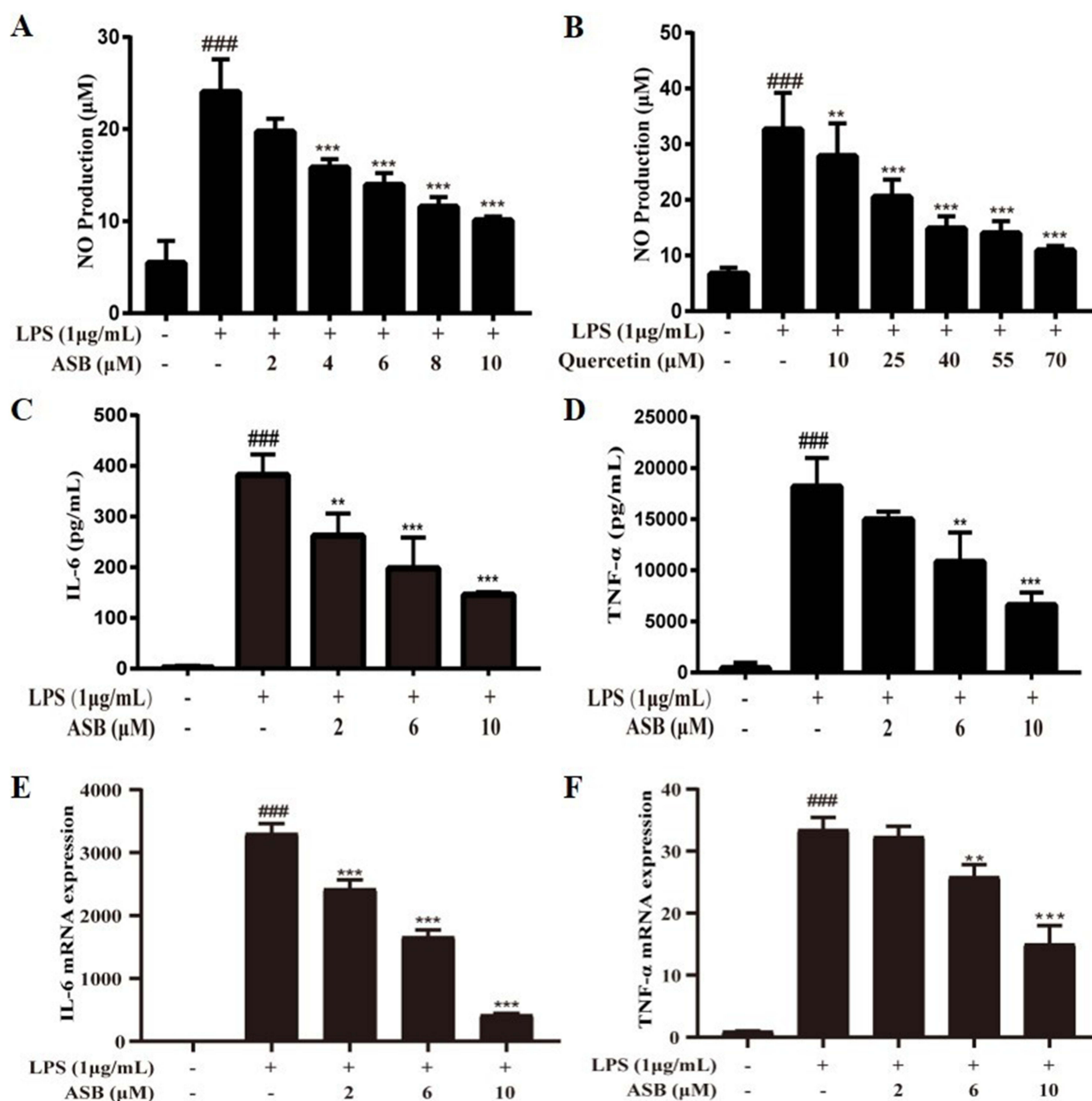
Figure 2 Effects of ASB on the levels of NO, IL-6 and TNF-α in LPS-stimulated RAW 264.7 macrophages. (**A** and **B**) The impact of ASB and quercetin on NO production was assessed using the Griess method. (**C** and **D**) The production of IL-6 and TNF-α were detected by ELISA. (**E** and **F**) The IL-6 and TNF-α mRNA expressions were determined by qRT-PCR. Data were displayed as means ± SD (n = 3). ###$P<0.001$ compared with the control group; **$P<0.01$, ***$P<0.001$ compared with the LPS-alone group.

ASB Suppressed the LPS-Induced Proinflammatory Cytokines Secretion and mRNA Expressions

The suppressing effects of ASB on the generation and mRNA expressions of proinflammatory cytokines IL-6 and TNF-α were further investigated in LPS-stimulated RAW 264.7 macrophages. As depicted in Figure 2C–F, ASB significantly suppressed the generation and mRNA expressions of IL-6 and TNF-α in a concentration-dependent manner.

ASB Restrained the LPS-Stimulated ROS Production

The impact of ASB on LPS-induced ROS generation was assessed using fluorescence microscopy and flow cytometry techniques. The findings demonstrated a significant dose-dependent suppression of LPS-induced ROS generation by ASB. The corresponding results were illustrated in Figure 3A–C.

ASB Inhibited the LPS-Induced iNOS and COX-2 Protein and mRNA Expressions

Subsequently, the LPS-induced iNOS and COX-2 protein and mRNA expressions were researched to further evaluate the anti-inflammatory activity of ASB. As illustrated in Figure 4A–C, ASB could intensely reduce the protein expressions of iNOS and COX-2 by LPS-induced in RAW 264.7 cells in a concentration-dependent manner. Moreover, the LPS-induced iNOS and COX-2 mRNA expressions were also decreased in a dose-dependent manner after undergoing ASB treatment (Figure 4D and E). The data suggest that ASB exerts a potent inhibitory effect on the LPS-induced inflammatory response.

ASB Had No Effects on the NF-κB Signaling Pathway

To reveal the potential mechanism of ASB in anti-inflammatory effect, the proteins expressions in the NF-κB pathway were initially assessed using Western blot technique. The outcomes demonstrated that LPS treatment remarkably induced the phosphorylation of AKT, NF-κB p65 and IκBα in RAW 264.7 cells in comparison to the control group. Nevertheless, ASB treatment did not block the phosphorylation of AKT, NF-κB p65 and IκBα induced by LPS (Figure 5A–D). Hence, the findings indicated that ASB did not have the capacity to modulate the NF-κB signaling pathway in order to manifest its anti-inflammatory properties.

ASB Modulated the MAPK and STATs Signaling Pathways

Next, we evaluated the impact of ASB on MAPK signaling pathway by evaluating the expression levels of p-p38, p-JNK and p-ERK. As illustrated in Figure 6A–D, p-p38, p-JNK and p-ERK expression levels were markedly increased in RAW
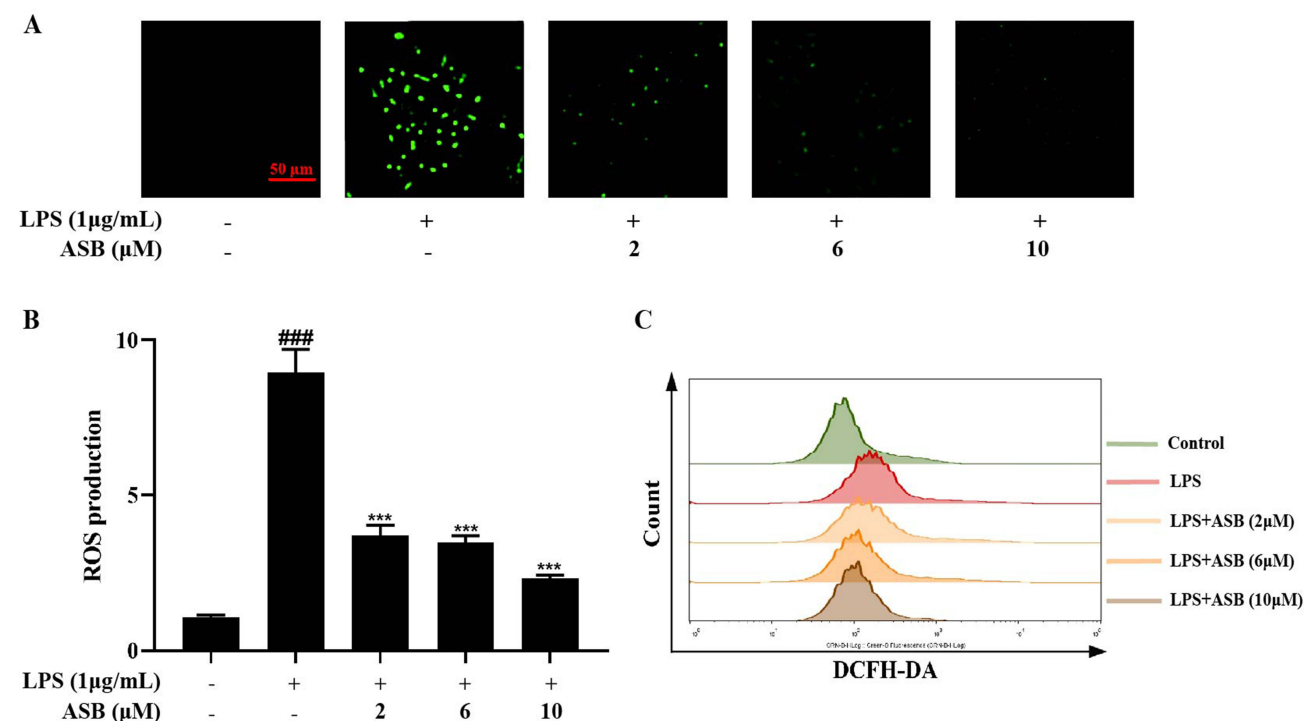

Figure 3 Effects of ASB on the LPS-induced ROS generation. (**A** and **B**) The ROS generation was assessed using fluorescence microscopy and quantified in LPS-stimulated RAW 264.7 macrophages. (**C**) The ROS was evaluated using flow cytometry in LPS-stimulated RAW 264.7 macrophages. Data were expressed as means ± SD (n = 3). ###P<0.001 compared with the control group; ***P<0.001 compared with the LPS-alone group.
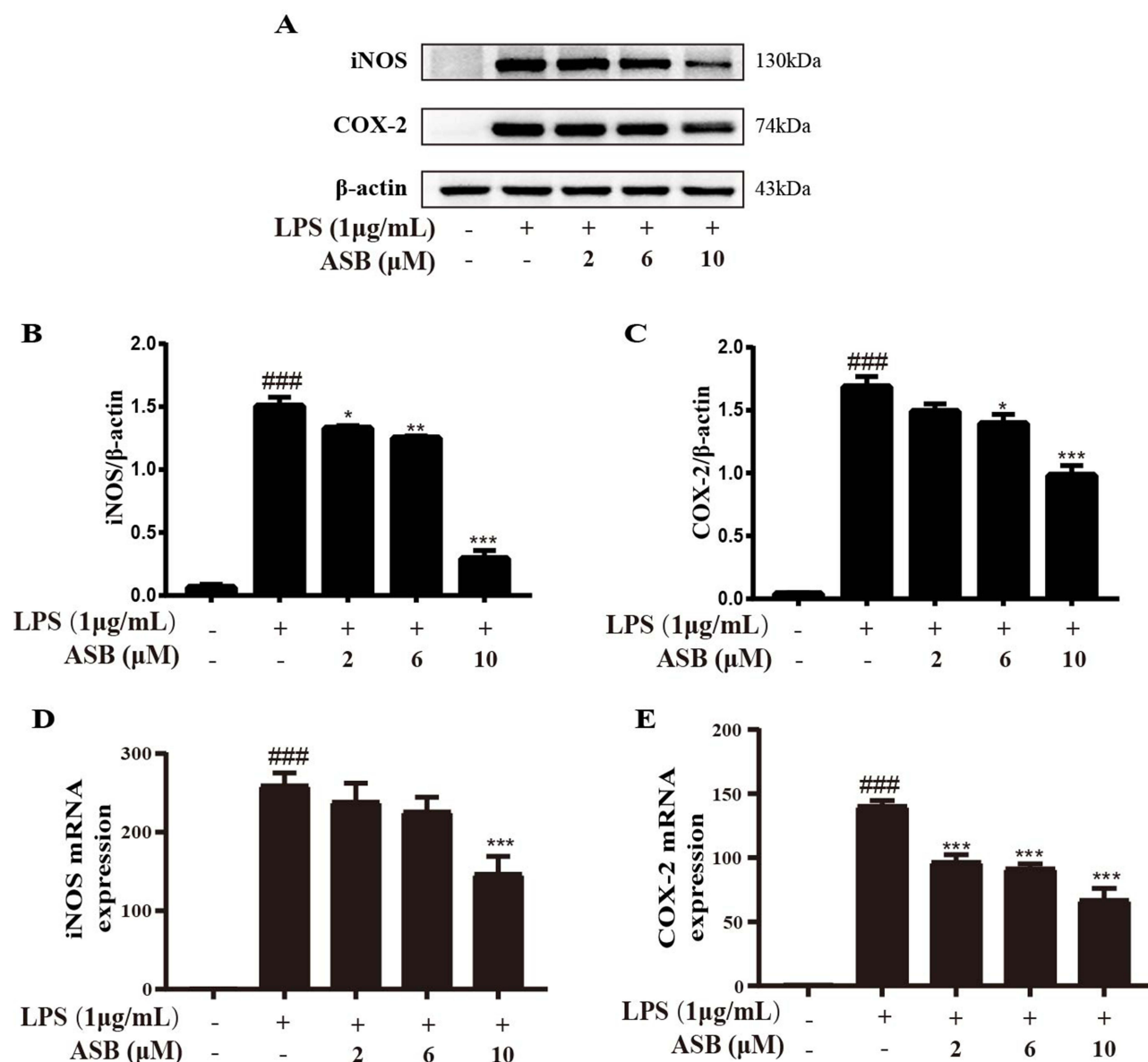
A

Figure 4 Effects of ASB on the LPS-induced iNOS and COX-2 protein and mRNA expressions. (**A–C**) The protein expressions of iNOS and COX-2 were investigated by Western blotting in LPS-stimulated RAW 264.7 macrophages. (**D** and **E**) The mRNA expressions of iNOS and COX-2 were investigated by qRT-PCR in LPS-stimulated RAW 264.7 macrophages. Data were presented as means ± SD (n = 3). ###$P<0.001$ compared with the control group; *$P<0.05$, **$P<0.01$, ***$P<0.001$ compared with the LPS-alone group.

264.7 macrophages by LPS-stimulating. After treatment with ASB, the expression of p-ERK and p-JNK were significantly decreased in a dose-dependent manner in comparison to LPS group, whereas the LPS-induced p-p38 expression was not restrained.

Moreover, the impact of ASB on the STATs signaling pathway was further assessed through an analysis of the expression levels of p-STAT1 and p-STAT3. The results displayed that the LPS-induced p-STAT3 high expression in RAW 264.7 cells were significantly inhibited in a dose-dependent manner by ASB treatment. Furthermore, ASB treatment could merely reduce the phosphorylation of STAT1 induced by LPS at 2 μM (Figure 7A–C). In order to further validate the impact of ASB on the STATs pathway induced by LPS, an immunocytochemical assay was conducted to assess the effect of ASB on STAT3 translocation. As illustrated in Figure 7D, the STAT3 protein (green) in the control cells were located outside the nucleus (blue) and was present in the cytoplasm. LPS greatly promoted STAT3
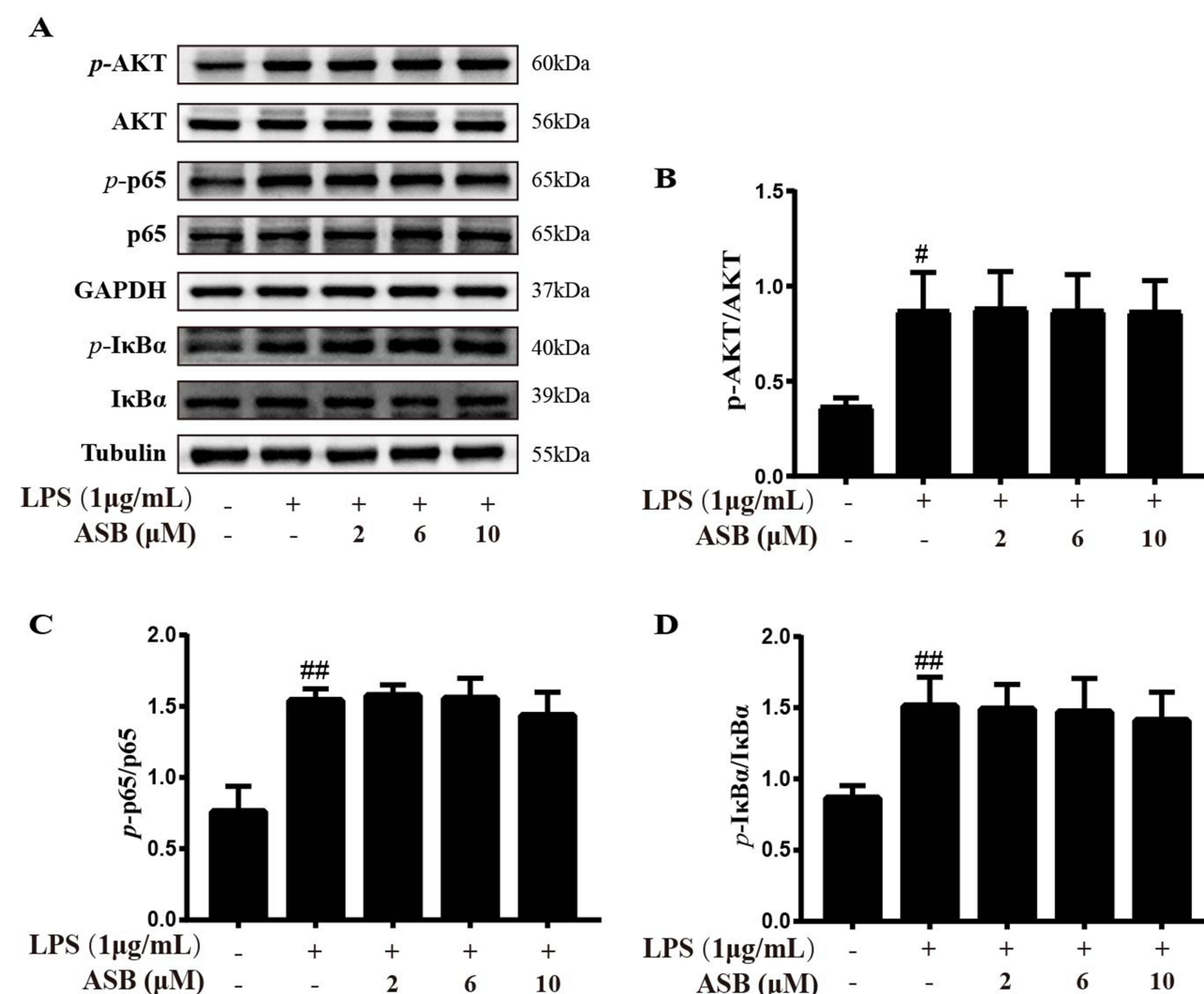
Figure 5 Effects of ASB on the NF-κB signaling pathway in LPS-induced RAW 264.7 macrophages. (**A**) The proteins of NF-κB pathway were analyzed by Western blotting. (**B–D**) The protein levels of *p*-AKT/AKT, *p*-p65/p65 and *p*-IκBα/IκBα. Data were expressed as means ± SD (n = 3). #*P*<0.05, ##*P*<0.01 compared with the control group.

translocation into the cell nucleus, while treatment with ASB (at 10 μM) could prevent the nuclear translocation of STAT3. The outcomes implied that ASB restrained the nuclear translocation of the cytoplasmic STAT3.

To sum up, ASB could block the phosphorylation of JNK, ERK, STAT1 and STAT3, and restrain the nuclear translocation of the cytoplasmic STAT3 in LPS-induced RAW 264.7 cells, which suggested that it could suppress the LPS-induced inflammatory response through the down-regulation of the MAPK and STATs signaling pathways.

Molecular Docking Results of ASB and the Target Proteins

A molecular docking analysis was performed to demonstrate the binding capacity of ASB with target proteins (ERK1, ERK2, JNK, STAT1 and STAT3), in order to illustrate its anti-inflammatory mechanism. The negative binding energy suggests the potential for the ligand molecule to bind with the receptor target protein. A higher absolute affinity value signifies that the active compound exhibits stronger binding affinity with the target protein.[17] In general, the binding energy between the tested compound and target protein was found to be below −5 kcal/mol, suggesting strong binding affinity and a stable conformation of the binding complex.[18] The molecular docking results between ASB and all targets are presented in Figure 8. In Figure 8A, it is evident that ASB exhibits robust binding activities with five target proteins, characterized by binding energies below −6.0 kcal/mol. The molecular docking interactions were visualized utilizing the PyMOL software (Figure 8B–F), showcasing the
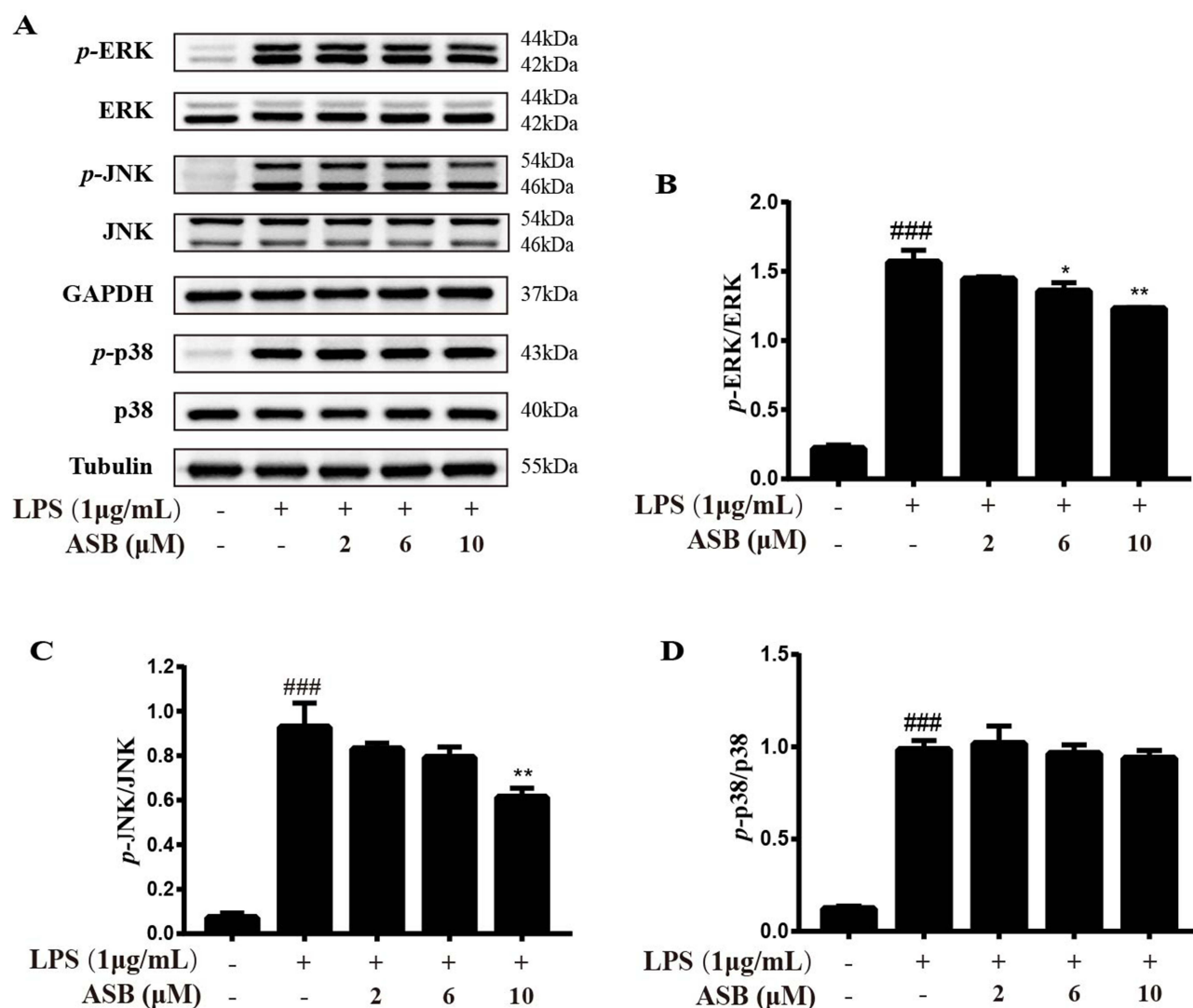
Figure 6 Effects of ASB on the MAPK signaling pathway in LPS-induced RAW 264.7 macrophages. (**A**) The proteins of MAPK pathway were analyzed by Western blotting. (**B–D**) The protein levels of p-ERK/ERK, p-JNK/JNK and p-p38/p38. Data were expressed as means ± SD (n = 3). $^{###}P<0.001$ compared with the control group; $^{*}P<0.05$, $^{**}P<0.01$ compared with the LPS-alone group.

predominant hydrogen bond interactions. The findings indicated that ASB showed robust binding affinity towards all target proteins, with the highest affinity observed for STAT3. Furthermore, molecular docking analysis provided additional evidence supporting the potential anti-inflammatory role of ASB through its targeted interaction with these proteins.

ASB Reduced the Level of ROS in CuSO₄-Induced Zebrafish

ROS, a crucial signaling molecule in the pathogenesis of inflammatory illnesses, is involved in the development of inflammatory response upon activation of inflammation.[19] Thus, we further examined the impact of ASB on ROS production in CuSO₄-induced zebrafish inflammatory model. First, the toxic potential of ASB in zebrafish was tested. The zebrafish larvae were exposed to ASB at concentrations of 10, 20, and 30 μM for a duration of 5 days, with daily monitoring of larval mortality. The result indicated that ASB exhibited no toxicity towards zebrafish larvae, as evidenced by a 100% survival rate at 8 dpf (Figure 9A). In the ROS evaluation experiment, CuSO₄ group induced a significantly increased fluorescence intensity of ROS in comparison to the control group, suggesting successful construction of the experimental model. Treatments with ASB (10, 20 and 30 μM) resulted in a significant concentration-dependent attenuation of ROS generation compared to the CuSO₄ group
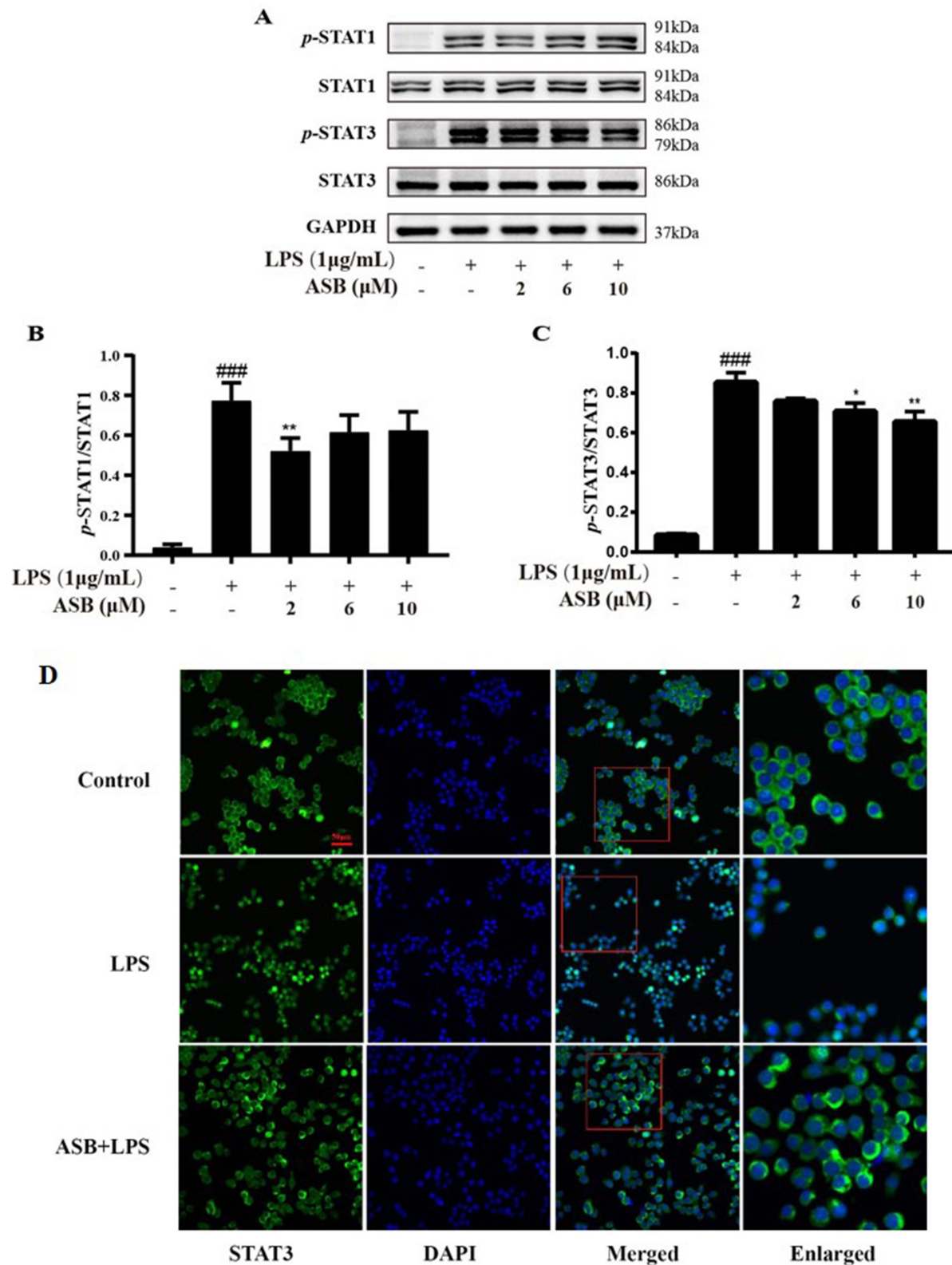
Figure 7 Effects of ASB on the STATs signaling pathway in LPS-induced RAW 264.7 macrophages. (**A**) The proteins of STATs pathway were analyzed by Western blotting. (**B** and **C**) The protein levels of *p*-STAT1/STAT1 and *p*-STAT3/STAT3. (**D**) Effect of ASB on STAT3 nuclear translocation was investigated by immunofluorescence assay. It was to show the double staining of STAT3 (in green) and DAPI (in blue) in cells (scale bar: 50 μm). Data were expressed as means ± SD (n = 3). [###]$P<0.001$ compared with the control group; [*]$P<0.05$, [**]$P<0.01$ compared with the LPS-alone group.
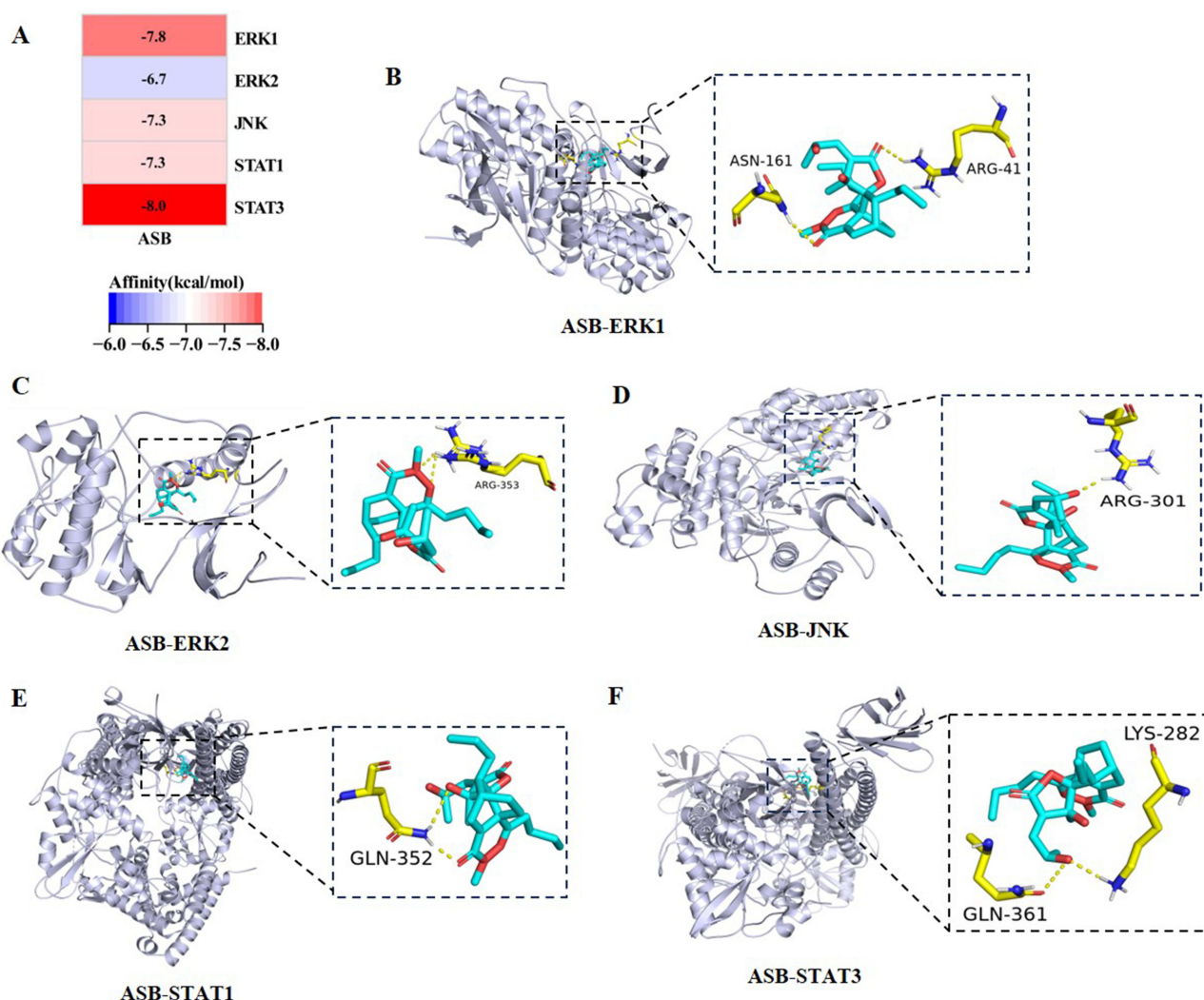
Figure 8 Molecular docking results of ASB and the target proteins. (**A**) Heatmap of the docking scores of ASB and the target proteins. (**B–F**) 3D graphs of molecular docking between ASB and the target proteins ((**B**) ASB-ERK1; (**C**) ASB-ERK2; (**D**) ASB-JNK; (**E**) ASB-STAT1; (**F**) ASB-STAT3).

(Figure 9B and C). This indicated that the ASB pretreatment had the potential to significantly mitigate $CuSO_4$-induced ROS production.

ASB Suppressed the $CuSO_4$-Induced Proinflammatory Cytokines mRNA Expressions in Zebrafish

In the subsequent experiment, the mRNA expressions of proinflammatory cytokines IL-6 and TNF-α were investigated in the inflammatory zebrafish model established by $CuSO_4$ treatment. As presented in Figure 9D and E, the mRNA expression levels of IL-6 and TNF-α were significantly elevated in the $CuSO_4$ group in comparison to the control group, which was markedly inhibited by ASB treatment. The findings demonstrated that ASB had the ability to effectively restrain the expressions of IL-6 and TNF-α in the inflammatory zebrafish.

Discussion

ASB, an unusual phthalide dimer featuring a peroxy bridge isolated from *A. sinensis* radix, with anticoagulation activity, has once been reported by our group. The anti-inflammatory potential of ASB had yet to be explored. Hence, in order to
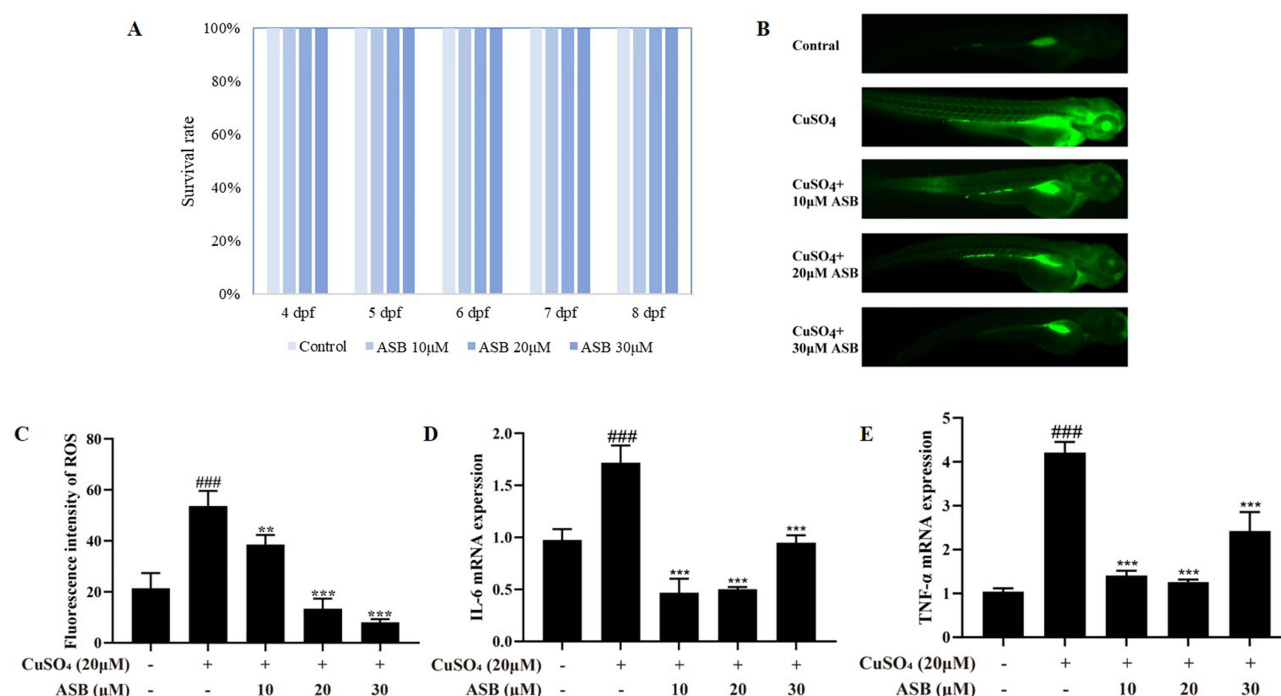
Figure 9 Effect of ASB on the CuSO₄-induced zebrafish inflammatory model. (**A**) The impact of ASB on the survival rate of zebrafish. (**B**) The generation of ROS in CuSO₄-induced zebrafish was determined using the fluorescent probe H2DCFDA. (**C**) Fluorescence intensity of ROS was quantified. (**D** and **E**) The pro-inflammatory cytokines IL-6 and TNF-α mRNA expressions were investigated by qRT-PCR in CuSO₄-induced zebrafish. Data were displayed as means ± SD (n = 3). $^{\#\#\#}P<0.001$ compared with the control group; $^{**}P<0.01$, $^{***}P<0.001$ compared with the model group.

elucidate its anti-inflammatory action and underlying mechanism, both in vitro and in vivo studies were undertaken in this investigation.

Inflammation serves as a crucial defense mechanism in safeguarding the human body against foreign pathogens. However, disproportionate or aberrant inflammatory reactions may precipitate diverse pathological conditions. Hence, the regulation of the inflammatory response holds significant implications for the management of interrelated diseases and the maintenance of overall health. Macrophages take a pivotal role in modulating inflammatory responses through the release of diverse inflammatory mediators and cytokines, including NO, TNF-α, IL-6, among others. An abundance of these inflammatory factors has the potential to induce both acute and chronic inflammatory states.[20–22] In particular, NO takes a crucial role in the regulation of immunity and maintenance of homeostasis; however, excessive generation of NO can give rise to a variety of inflammation-related diseases. As such, NO is considered to be a hopeful target for the management of inflammatory conditions.[23–25] This study showed that ASB could inhibit the generation of NO induced by LPS in RAW 264.7 cells with an IC$_{50}$ value of 4.98 ± 0.94 μM. Its inhibitory capability was more potent than that of positive control quercetin (IC$_{50}$ value of 26.06 ± 2.28 μM). When exposed to external pathogens and LPS, macrophages release substantial quantities of proinflammatory cytokines TNF-α and IL-6, which subsequently promote the upregulation of iNOS in inflammatory cells, leading to an elevation in NO release. TNF-α and IL-6 are crucially involved in the initiation of inflammatory processes.[26,27] Our study demonstrated that ASB could significantly inhibit the secretion and mRNA expression of proinflammatory cytokines IL-6 and TNF-α in RAW264.7 macrophages induced by LPS.

Macrophages are capable of producing proinflammatory mediators such as NO and prostaglandin E2 through iNOS and COX-2, respectively, in addition to cytokines including TNF-α and IL-6, thereby promoting the onset of an inflammatory response.[28] iNOS, an isoform of NO synthase, facilitates the generation of NO upon cellular stimulation. COX-2, a pivotal enzyme in prostaglandin biosynthesis, orchestrates the biosynthesis of prostaglandin E2 from arachidonic acid.[4,29] Our study revealed that ASB could inhibit the protein and mRNA levels of iNOS and COX-2 induced by LPS in RAW264.7 macrophages.

ROS is involved in the modulation of inflammatory response through various inflammatory pathways. The clearance of ROS is crucial in preventing excessive inflammatory responses. Therefore, targeting the regulation of ROS and related pathways may be regarded as a novel approach for the management of inflammatory conditions. The results demonstrated the inhibitory action of ASB on ROS generation induced by LPS in RAW264.7 cells.

The LPS-induced inflammatory response is orchestrated through an intricate web of inflammatory signaling cascades, including NF-κB, MAPK, STATs, and other pathways.[30–32] NF-κB, a crucial inflammatory pathway, is considered to be the familiar signaling pathway in orchestrating inflammatory response.[2,33] In the RAW 264.7 cells, LPS induced high expressions of p-IκBα, p-p65 and p-AKT were not reversed by ASB treatment, which suggested that ASB did not inhibit LPS-stimulated inflammatory response through modulating the NF-κB signaling pathway. MAPK, a kinase family that includes ERK, p38 and JNK, has been associated with the transcriptional regulation for COX-2, iNOS and inflammatory cytokines during the process of inflammation.[34–36] Hence, the impact of ASB on the MAPK pathway was further scrutinized. The findings of this investigation revealed that ASB effectively suppressed the phosphorylation of ERK1/2 and JNK induced by LPS, indicating its anti-inflammatory properties through modulation of the MAPK pathways. The STAT protein is a crucial intracellular signaling and transcriptional activation cytokine. Both STAT1 and STAT3 have the ability to trigger inflammation through diverse pathways, with the STAT signaling pathway playing a crucial role throughout the entire inflammatory process, encompassing initiation, progression, and resolution.[37,38] Our results displayed that LPS-induced phosphorylation of STAT1 and STAT3 were conspicuously suppressed with ASB treatment. Moreover, ASB prevented the nuclear translocation of STAT3 in LPS-activated RAW264.7 macrophages. Based on the aforementioned findings, it is proposed that ASB demonstrates anti-inflammatory properties through modulation of the MAPK and STATs signaling pathways.

The molecular mechanism of ASB against inflammation was further verified by molecular docking. Molecular docking analysis uncovered that ASB exhibited high affinities towards the target proteins (ERK1, ERK2, JNK, STAT1 and STAT3) in the MAPK and STATs signaling pathways, among which STAT3 had the highest affinity. It can be seen that the MAPK and STATs signaling pathways play a key role for anti-inflammatory molecular mechanism of ASB.

The anti-inflammatory efficacy of ASB was further confirmed in an in vivo setting. In the inflammatory zebrafish model induced by $CuSO_4$, ASB treatment effectively attenuated the excessive generation of ROS and diminished the
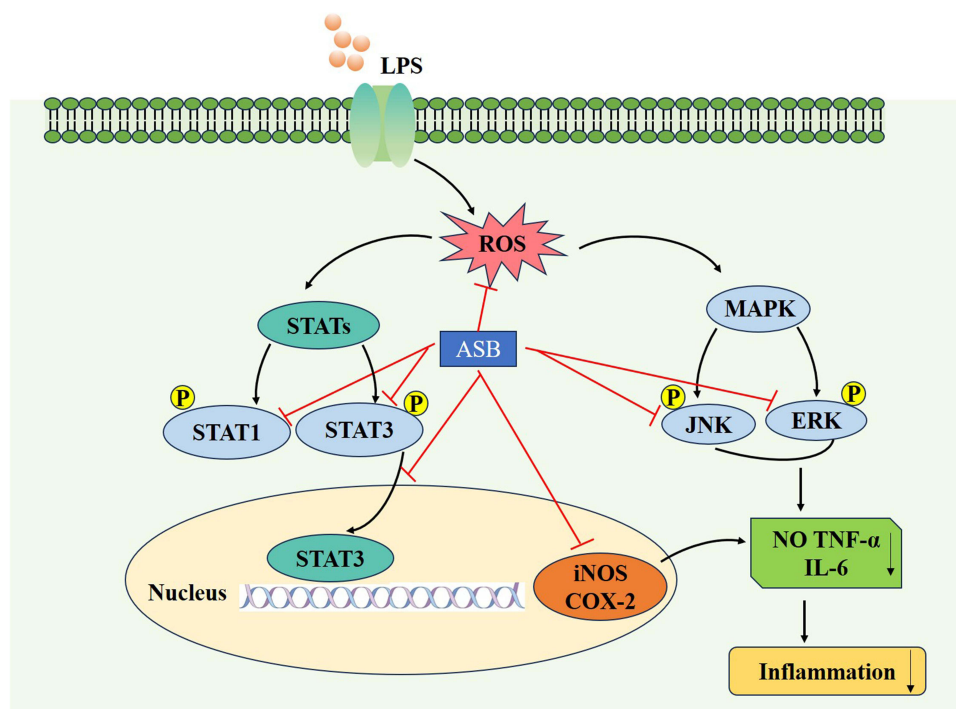

Figure 10 Anti-inflammatory mechanism of ASB in RAW 264.7 macrophages.

high mRNA expression levels of IL-6 and TNF-α. The findings demonstrated the significant in vivo anti-inflammatory effectiveness of ASB.

ASB is the sole phthalide dimer peroxy compound, and this study represents the first exploration of the anti-inflammatory function of ASB. Our studies reveal that ASB demonstrates a remarkable anti-inflammatory effect both in vivo and in vitro. The mechanism might be associated with the down-regulation of MAPK and STATs signaling pathways and the inhibition of ROS production. It is anticipated that ASB will serve as an efficacious treatment for inflammation-related disorders. However, there exists certain limitation in this study. The mechanism in vivo remains insufficiently investigated and requires further exploration.

Conclusion

In conclusion, ASB could significantly exert a remarkable anti-inflammatory efficacy through inhibiting the release of NO, IL-6 and TNF-α in LPS-stimulated RAW264.7 macrophages, restraining the ROS generation, suppressing the protein and mRNA expressions of iNOS and COX-2, and also down-regulating MAPK and STATs signaling pathways (Figure 10). Molecular docking results further validated the anti-inflammatory properties of ASB by targeting MAPK and STATs signaling pathways. Furthermore, ASB could significantly decrease the excessive generation of ROS and the mRNA overexpression of IL-6 and TNF-α in the inflammatory zebrafish model induced by $CuSO_4$. Collectively, these findings demonstrate the pronounced anti-inflammatory effectiveness of ASB both in vitro and in vivo. This study serves as a foundation for the potential utilization of ASB in the anti-inflammatory medications or functional food products. However, the in vivo anti-inflammatory mechanism in this study is not comprehensive enough and requires further exploration in the future.

Author Contributions

All authors made a significant contribution to the work reported, whether that is in the conception, study design, execution, acquisition of data, analysis and interpretation, or in all these areas; took part in drafting, revising or critically reviewing the article; gave final approval of the version to be published; have agreed on the journal to which the article has been submitted; and agree to be accountable for all aspects of the work.

Funding

Disclosure

The authors declare no conflicts of interest in this work.

References

1. Lee HH, Shin JS, Chung KS. et al. 3′,4′-Dihydroxyflavone mitigates inflammatory responses by inhibiting LPS and TLR4/MD2 interaction. *Phytomedicine*. 2023;109:154553. doi:10.1016/j.phymed.2022.154553
2. Yang M, Wang Y, Fan Z, et al. Chemical constituents and anti-inflammatory activity of the total alkaloid extract from *Melodinus cochinchinensis* (Lour.) Merr. and its inhibition of the NF-κB and MAPK signaling pathways. *Phytomedicine*. 2021;91:153684. doi:10.1016/j.phymed.2021.153684
3. Lee HS, Kwon YJ, Seo EB, et al. Anti-inflammatory effects of *Allium cepa* L. peel extracts via inhibition of JAK-STAT pathway in LPS-stimulated RAW264.7 cells. *J Ethnopharmacol*. 2023;317:116851. doi:10.1016/j.jep.2023.116851
4. Wang F, Liu L, Zhu Z, et al. Anti-inflammatory effect and mechanism of active parts of *Artemisia mongolic*a in LPS-induced Raw264.7 cells based on network pharmacology analysis. *J Ethnopharmacol*. 2024;321:117509. doi:10.1016/j.jep.2023.117509
5. Li JJ, Zhang Y, Han LW, et al. Tenacissoside H exerts an anti-inflammatory effect by regulating the nf-κb and p38 pathways in zebrafish. *Fish Shellfish Immunol*. 2018;83:205–212. doi:10.1016/j.fsi.2018.09.032
6. Bin XN, Gao YB, Pan M, et al. Anti-inflammatory effects of 6S-5-methyltetrahydrofolate-calcium on RAW264.7 cells and zebrafish. *Life Sci*. 2023;327:121839. doi:10.1016/j.lfs.2023.121839
7. Zanandrea R, Bonan CD, Campos MM. Zebrafish as a model for inflammation and drug discovery. *Drug Discov Today*. 2020;25(12):2201–2211. doi:10.1016/j.drudis.2020.09.036
8. Wei X, Zeng Y, Sun C, et al. Recent advances in natural phthalides: distribution, chemistry, and biological activities. *Fitoterapia*. 2022;160:105223. doi:10.1016/j.fitote.2022.105223

9. Huang L, Peng C, Guo L, et al. Six pairs of enantiomeric phthalide dimers from the rhizomes of *Ligusticum chuanxiong* and their absolute configurations and anti-inflammatory activities. *Bioorg Chem*. 2022;127:105970. doi:10.1016/j.bioorg.2022.105970

10. He YW, Liu XQ, Chen K, et al. New dimeric phthalides from the rhizomes of *Ligusticum sinense* Oliv. *Fitoterapia*. 2021;150:104837. doi:10.1016/j.fitote.2021.104837

11. Lv JL, Zhang LB, Guo LM. Phthalide dimers from *Angelica sinensis* and their COX-2 inhibition activity. *Fitoterapia*. 2018;129:102–107. doi:10.1016/j.fitote.2018.06.016

12. Lyu CL, Li HH, Shi YJ, et al. Research progress of Angelicae Sinensis Radix and predictive analysis on its quality markers. *China J Chin Mater Med*. 2022;47(19):5140–5157. doi:10.19540/j.cnki.cjcmm.20220225.203

13. Zhang LB, Lv JL, Liu JW. Phthalide Derivatives with Anticoagulation Activities from *Angelica sinensis*. *J Nat Prod*. 2016;79(7):1857–1861. doi:10.1021/acs.jnatprod.6b00080

14. Zhang LB, Guo LM, Wang FL, et al. Phytochemical Profile and Anti-Inflammatory Activity of the Fraction from *Artemisia lavandulaefolia*. *Chem Biodiv*. 2021;18(3):e2000989. doi:10.1002/cbdv.202000989

15. Zhang LB, Zhu HH, Guo LM, et al. Artemargyinolide E, a new sesquiterpene lactone from *Artemisia argyi* inhibits inflammatory responses via down-regulating NF-κB signaling pathway. *Phytochem Let*. 2020;36:17–23. doi:10.1016/j.phytol.2020.01.009

16. Liu N, Zhang P, Xue M, et al. Anti-inflammatory and antioxidant properties of rice bran oil extract in copper sulfate-induced inflammation in zebrafish (*Danio rerio*). *Fish Shellfish Immunol*. 2023;136:108740. doi:10.1016/j.fsi.2023.108740

17. Sun Z, Wang Y, Pang X, et al. Mechanisms of polydatin against spinal cord ischemia–reperfusion injury based on network pharmacology, molecular docking and molecular dynamics simulation. *Bioorg Chem*. 2023;140:106840. doi:10.1016/j.bioorg.2023.106840

18. Yu Z, Wu Y, Ma Y, et al. Systematic analysis of the mechanism of aged citrus peel (Chenpi) in oral squamous cell carcinoma treatment via network pharmacology, molecular docking and experimental validation. *J Funct Foods*. 2022;91:105012. doi:10.1016/j.jff.2022.105012

19. Ko EY, Cho SH, Kwon SH, et al. The roles of NF-κB and ROS in regulation of pro-inflammatory mediators of inflammation induction in LPS-stimulated zebrafish embryos. *Fish Shellfish Immunol*. 2017;68:525–529. doi:10.1016/j.fsi.2017.07.041

20. Hassan S, Sajjad N, Khan SU, et al. *Dipsacus inermis* Wall. modulates inflammation by inhibiting NF-κB pathway: an in vitro and in vivo study. *J Ethnopharmacol*. 2020;254:112710. doi:10.1016/j.jep.2020.112710

21. Chen J, Li DL, Xie LN, et al. Synergistic anti-inflammatory effects of silibinin and thymol combination on LPS-induced RAW264.7 cells by inhibition of NF-κB and MAPK activation. *Phytomedicine*. 2020;78:153309. doi:10.1016/j.phymed.2020.153309

22. Li SS, Li J, Sun J, et al. Berkeleyacetal C, a meroterpenoid isolated from the fungus Penicillium purpurogenum MHZ111, exerts anti-inflammatory effects via inhibiting NF-κB, ERK1/2 and IRF3 signaling pathways. *Eur J Pharmacol*. 2017;814:283–293. doi:10.1016/j.ejphar.2017.08.039

23. Wang R, Zeng J, Chen L, et al. Diterpenoid WT-29 isolated from Wedelia exerted anti-inflammatory and anti-allergic activities. *J Ethnopharmacol*. 2024;319:117265. doi:10.1016/j.jep.2023.117265

24. Liu W, Wu P, Song Z, et al. Iridoids from *Patrinia heterophylla* and their anti-inflammatory activity. *Phytochemistry*. 2023;212:113720. doi:10.1016/j.phytochem.2023.113720

25. Huang Y, Wang Y, Xu J, et al. Propacin, a coumarinolignoid isolated from durian, inhibits the lipopolysaccharide-induced inflammatory response in macrophages through the MAPK and NF-κB pathways. *Food Funct*. 2020;11(1):596–605. doi:10.1039/c9fo02202c

26. Zhao Q, Zheng W, Yuan Z, et al. Anti-inflammatory effect of two novel peptides derived from Binglangjiang Buffalo whey protein in lipopolysaccharide-stimulated RAW264.7 macrophages. *Food Chem*. 2023;429:136804. doi:10.1016/j.foodchem.2023.136804

27. Singh P, Kaur S, Sharma A, et al. TNF-α and IL-6 inhibitors: conjugates of N-substituted indole and aminophenylmorpholin-3-one as anti-inflammatory agents. *Eur J Med Chem*. 2017;140:92–103. doi:10.1016/j.ejmech.2017.09.003

28. Kang E, Lee J, Seo S, et al. Regulation of anti-inflammatory and antioxidant responses by methanol extract of *Mikania cordata* (Burm. f.) B. L. Rob. leaves via the inactivation of NF-κB and MAPK signaling pathways and activation of Nrf2 in LPS-induced RAW 264.7 macrophages. *Biomed Pharmacother*. 2023;168:115746. doi:10.1016/j.biopha.2023.115746

29. Ardizzone S, Porro GB. Biologic therapy for inflammatory bowel disease. *Drugs*. 2005;65(16):2253–2286. doi:10.2165/00003495-200565160-00002

30. Nardo DD. Toll-like receptors: activation, signalling and transcriptional modulation. *Cytokine*. 2015;74(2):181–189. doi:10.1016/j.cyto.2015.02.025

31. Jeong JW, Lee HH, Han MH, et al. Anti-inflammatory effects of genistein via suppression of the toll-like receptor 4-mediated signaling pathway in lipopolysaccharide-stimulated BV2 microglia. *Chem Biol Interact*. 2014;212:30–39. doi:10.1016/j.cbi.2014.01.012

32. Kim EA, Kim SY, Kim J, et al. Tuberatolide B isolated from Sargassum macrocarpum inhibited LPS-stimulated inflammatory response via MAPKs and NF-κB signaling pathway in RAW264.7 cells and zebrafish model. *J Funct Foods*. 2019;52:109–115. doi:10.1016/j.jff.2018.10.030

33. Lu XG, Min L, Wei JL, et al. Heliangin inhibited lipopolysaccharide-induced inflammation through signaling NF-κB pathway on LPS-induced RAW 264.7 cells. *Biomed Pharmacother*. 2017;88:102–108. doi:10.1016/j.biopha.2017.01.041

34. Li X, Hu Y, He B, et al. Design, synthesis and evaluation of ursodeoxycholic acid-cinnamic acid hybrids as potential anti-inflammatory agents by inhibiting Akt/NF-κB and MAPK signaling pathways. *Eur J Med Chem*. 2023;260:115785. doi:10.1016/j.ejmech.2023.115785

35. Hou XL, Tong Q, Wang WQ, et al. Suppression of inflammatory responses by dihydromyricetin, a flavonoid from *Ampelopsis grossedentata*, via inhibiting the activation of NF-κB and MAPK signaling pathways. *J Nat Prod*. 2015;78(7):1689–1696. doi:10.1021/acs.jnatprod.5b00275

36. Seo KH, Park MJ, Ra JE, et al. Saponarin from barley sprouts inhibits NF-κB and MAPK on LPS-induced RAW 264.7 cells. *Food Funct*. 2014;5(11):3005–3013. doi:10.1039/c4fo00612g

37. Kim HJ, Song HK, Park SH, et al. *Terminalia chebula Retz*. extract ameliorates the symptoms of atopic dermatitis by regulating anti-inflammatory factors *in vivo* and suppressing STAT1/3 and NF-κB signaling in vitro. *Phytomedicine*. 2022;104:154318. doi:10.1016/j.phymed.2022.154318

38. Loh CY, Arya A, Naema AF, et al. Signal transducer and activator of transcription (STATs) proteins in cancer and inflammation: functions and therapeutic implication. *Front Oncol*. 2019;9:48. doi:10.3389/fonc.2019.00048